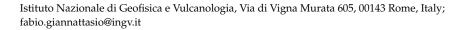




Editorial

Ionosphere Monitoring with Remote Sensing

Fabio Giannattasio 🗅



1. Introduction

Characterising the physical properties of the Earth's ionosphere is fundamental to shed light on the dynamic processes occurring therein on a wide range of both spatial and temporal scales and to understand several phenomena relevant to Space Weather.

In fact, due to the presence of ions and electrons, the ionosphere reacts to the onset, amplification and evolution of magnetic and electric fields.

This response may substantially change the physical properties of the ionosphere and its energetic budget and may be reflected, for example, in the modification of the propagation properties of electromagnetic signals traveling through the ionospheric medium.

Due to the conspicuous amount of high-quality data, these features can be reliably investigated at different scales taking advantage of remote sensing and in situ facilities such as ionosondes, radars, satellites and Global Navigation Satellite Systems (GNSS) receivers.

2. Overview of Contribution and Future Perspectives

In this context, the Special Issue "Ionosphere Monitoring with Remote Sensing" aims at promoting significant advances in our knowledge of the ionosphere through the use of different data from different facilities as well as currently recognized ionospheric models. In fact, the Special Issue focuses on: (1) the investigation of the impact of sunlit, solar and geomagnetic activity on the ionosphere at all latitudes; (2) the investigation of the impact of ionospheric variations on contemporary technology; (3) the improvement of ionospheric models through new instrumental observations, analyses and data-handling techniques; (4) the investigation of magnetosphere—ionosphere coupling through multi-instrumental approaches; and (5) the promotion of new instruments, missions and tools to monitor the ionosphere.

The Special Issue provides 15 original research papers describing results obtained with a wide range of tools, data and analysis techniques and focused on the characterisation of several properties of the ionosphere.

As mentioned above, great attention has been paid to the development of new facilities and analysis techniques to increase our knowledge of the ionosphere. Shindin et al. [1] presented a prototype of a low-cost and good-quality fast ionosonde capable of performing with the unprecedented speed of one second cadence, which allows recording fast quasiperiodic and moving ionospheric disturbances in the F, E and Es layers. An additional strength is that the ionosonde is equipped with cheap, publicly available components, which favours the multi-position registration of ionograms and, as a consequence, the investigation of ionospheric disturbances in a three-dimensional region of space and the possibility to create a network of observation points. A layer of critical importance for ionospheric studies is the transition region between the lower and upper atmosphere, namely, the sporadic E (Es) layer, which consists of a region of enhanced ion plasma at altitudes between 90 and 120 km with a vertical extent of several kilometres and a horizontal extension of tens of kilometres [2]. The existence of this region can be explained by the wind shear theory and the convergence of metal ions and can be influenced by shear instabilities, tidal, planetary or gravity waves, meteors and thunderstorms [3–8]. The vertical structure of the Es layer is



Citation: Giannattasio, F. Ionosphere Monitoring with Remote Sensing. *Remote Sens.* **2022**, *14*, 5325. https://doi.org/10.3390/rs14215325

Received: 13 October 2022 Accepted: 21 October 2022 Published: 25 October 2022

Publisher's Note: MDPI stays neutral with regard to jurisdictional claims in published maps and institutional affiliations.



Copyright: © 2022 by the author. Licensee MDPI, Basel, Switzerland. This article is an open access article distributed under the terms and conditions of the Creative Commons Attribution (CC BY) license (https://creativecommons.org/licenses/by/4.0/).

Remote Sens. 2022, 14, 5325 2 of 8

still poorly understood due to its transient and complex nature together with limitations in observation techniques [9–13]. Liu et al. [14] applied the frequency domain interferometry (FDI) technique by using the Es layer measurements near Wuhan, China, on 8 June 2021. They pointed out that this technique allowed them to obtain increased spatial resolution of ionosonde imaging capable of identifying different types of Es and to capture its internal fine structure. Unlike the "classic" vertical sounding mode, for the oblique sounding mode, the transmitter and the receiver are located at stations that can be hundreds or thousands of kilometres apart [15–18]. The resulting oblique ionograms can capture ionospheric properties at the reflection point, which is usually located at the middle point between the transmitter and receiver. However, the problem of how to automatically scale oblique ionograms is still open, and various solutions have been identified over the years [19–23]. Jiang et al. [24] developed a method to carry out the automatic inversion of oblique ionograms to extract the parameters of the ionosphere together with the electron density profile. Their results show that the accuracy of the inferred autoscaled maximum observable frequency and minimum group path of the ordinary trace of the F2 layer is about 91.98% and 86.41%, respectively. Kim et al. [25] used Vertical Incidence Pulsed Ionospheric Radar (VIPIR) to observe the polar ionosphere with Dynasonde analysis software at Jang Bogo Station (74.6°S, 164.2°E), Antarctica, which is located in the polar cap, cusp or auroral oval depending on the local time and the geomagnetic activity conditions. The resulting F2-layer peak electron density (NmF2) and bottomside total electron content (TEC) exhibit an overall good correlation with GPS TEC measurements during quiet conditions. During the daytime and in summer, the bottomside TEC is less correlated with the GPS TEC due to particle precipitation and the onset of large density irregularities in the polar ionosphere. However, the Dynasonde analysis show some limitations and needs to be improved in order to provide accurate density profiles, especially during disturbed geomagnetic conditions. The use of radar imaging and interferometry techniques also provides important information on the physical properties of the ionosphere. In a horizontally structured atmosphere, radar echoes are strongest near the zenith and decrease with the angle off the zenith. In the presence of ionospheric field-aligned plasma irregularities (FAIs), radar echoes are strongest at the beam direction perpendicular to the geomagnetic field, with a fast decrease in the angle off the perpendicular direction. The aspect angle, which is a measure of the aspect sensitivity, i.e., the half width of half power or the standard deviation of Gaussian fitting in the angular power distribution, is of the order of degrees [26,27]. On the contrary, it can be of order 0.1 degrees or less in FAI echoes (see, e.g., Kudeki and Farley [28]). A way to effectively measure an FAI's aspect angle lies in the radar interferometry technique [28,29]. Chen et al. [30] applied the coherent radar imaging (CRI) technique to estimate the aspect angle of mid-latitude E region FAIs. CRI requires the use of separate antennas as independent receiving channels to collect radar echoes [27,31]. The echoes received allow one to retrieve the in-beam angular power distribution. By using the multireceiver and multifrequency capabilities of the 46.5 MHz middle and upper atmosphere radar in Japan, Chen et al. [30] showed that, among the three methods (namely, Fourier, Capon and norm-constrained Capon) used to recover the brightness distribution, the norm-constrained Capon method produces more reliable results and more trustworthy aspect angle values consistent with those obtained with the RI technique. Their results may help to shed light on the spatial and temporal properties of plasma irregularities in the ionosphere.

Karpachev [32] separated and classified ionospheric troughs (regions of anomalously decreased electron density) in the winter ionosphere of the Southern hemisphere by using CHAMP satellite data during high solar activity (between 2000 and 2002). In particular, the authors identified two kinds of high-latitude troughs: (1) a wide trough associated with a region of particle precipitation on the poleward edge of the auroral oval; (2) a narrow trough of ionisation presumably associated with an electric field. Moreover, the main ionospheric trough (MIT) was separated from the ring ionospheric trough (RIT), the latter being formed by the decay of the magnetospheric ring current.

Remote Sens. 2022, 14, 5325 3 of 8

A relevant aspect at the centre of ionospheric investigation concerns plasma density irregularities, which play a key role in the propagation of electromagnetic signals, being a cause of disturbance for the GNSS. In fact, irregularities are responsible for degradation and, eventually, interruptions in the signals received by the system. In the equatorial F region, irregularities are also known as plasma bubbles and develop on the nightside [33] at magnetic latitudes up to 20° in both hemispheres [34], at heights up to 1000–1550 km [35] and on a wide range of spatial scales, from hundreds of kilometres down to a few decametres [36]. Their spatial and temporal distribution depends on solar and geomagnetic activity and exhibits a diurnal and seasonal variation [33,37,38]. The origin of plasma bubbles is recognised to be due to the establishment of density gradients sufficient to trigger a Rayleigh–Taylor instability growth mechanism [34,39]. The irregularities generated in this way expand vertically and then follow the geomagnetic field lines in both directions above and below the magnetic equator. This dynamic is typically overlaid by an eastward drift motion due to polarising electric fields generated by neutral zonal winds. The instability of these structures can, in turn, generate secondary irregularities and trigger a cascading process. Several studies have pointed out the turbulent nature of plasma bubbles [40–45]. In this context, De Michelis et al. [46] focused on the relationship between the spectral features of electron density and magnetic field strength inside plasma bubbles in order to understand whether it is possible to study the dynamical features of plasma bubbles by using either the magnetic field or the electron density measurements. This is motivated by the fact that, in the past, important plasma bubble features have been detected by analysing their magnetic signatures using the diamagnetic effect [47]. However, studying plasma bubbles by using only magnetic field data may not be the correct way, as it implies that the scaling properties of electron density and magnetic fields are equal. To address this point, De Michelis et al. [46] studied the scaling properties of both electron density and magnetic fields associated with plasma bubbles using about two years of Swarm measurements at 1 Hz. Specifically, they applied the local detrended structure function analysis [48] and found that a complex relation may exist between the spectral features of electron density and magnetic field that depends on local time and latitude due to the evolution and turbulent nature of plasma bubbles. A more in-depth study of diamagnetic currents at high latitudes obtained by Swarm measurements has been performed by Lovati et al. [49]. Such weak currents are driven by pressure gradients and produce a magnetic field that is directed opposite to the background geomagnetic field and causes its reduction. The authors used 4 years of electron density, electron temperature and magnetic field data at 1 Hz to investigate the dependence of diamagnetic currents on local time, season, solar and geomagnetic activity and sunlit conditions. They confirmed the enhancement of diamagnetic currents at high latitudes, around the cleft region, during disturbed periods due to the increase in plasma pressure gradients. In the polar cap, currents flow regardless of the geomagnetic activity due to plasma instabilities driving irregularities and pressure gradients. Moreover, during disturbed periods, features in the correspondence of the auroral oval move to lower latitudes. These findings may help to improve current geomagnetic field models and understand the impact of ionospheric irregularities on dynamics at spatial scales of tens of kilometres.

New insights into dynamic processes in the ionosphere are obtained by studying its turbulent nature, which underlies, for example, chaotic plasma behaviour. The turbulent dynamics of ionospheric plasma has long been established, especially at high latitudes, by investigating, for example, fluctuations in magnetic and electric fields and electron density. Such fluctuations are characterised by power-law spectral densities, scaling features and non-Gaussian statistics of increments at all scales (see, e.g., [50–53]) and can affect plasma dynamics via the ExB drift term. At both high and low latitudes, variations in vertical plasma velocity drift plays a key role in the generation of irregularities [54–56]. In light of this, Consolini et al. [57] used electric and magnetic field measurements provided by the Chinese Seismo-Electromagnetic Satellite (CSES-01) to investigate the properties of the plasma ExB drift velocity during a crossing of the Southern auroral F region. Specifically,

Remote Sens. 2022, 14, 5325 4 of 8

they analysed the spectral and scaling features of velocity fluctuations and pointed out the turbulent nature of the drift. In more detail, the authors provided evidence of 2D intermittent turbulence at scales from tens of meters to tens of kilometres. This is consistent with filamentary or thin-tube-like features.

One of the most important application issues is the risk assessment of the impact that ionospheric variations may have on technology. A proper risk assessment allows the development of effective mitigation strategies. For example, ionospheric anomalies may result in potential threats for the ground-based augmentation system (GBAS), which is an airport-based augmentation of the GNSS capable of providing advanced civil-aviation services. When GNSS signals travel through ionospheric regions with enhanced gradients, severe errors may be observed and compromise the reliability of the GBAS. Thus, it is fundamental to quickly detect anomalies. In this context, Gao et al. [58] developed a monitor to clearly detect anomalies with an average detection speed improved by more than 16% when dealing with real data instead of simulations. Valdés-Abreu et al. [59] studied the effects of an annular solar eclipse on GNSS position estimation accuracy based on TEC measurements performed by over 2000 stations worldwide, which were validated with measurements by the Swarm satellite mission and four digisondes in Central and South America. In particular, TEC maps pointed out a TEC depletion under the moon's shadow and important variations in both crests of the Equatorial Ionization Anomaly (EIA). Variations typically affect the amplitude of the signal and its delay (see Bravo et al. [60] and references therein) and can affect regions outside the umbra and penumbra of the eclipse [61–63]. With this global coverage, the work of Valdés-Abreu et al. [59] allowed them to find other locations in the world that could be affected by perturbations in the North Pole and infer how that perturbations propagate to those potential locations.

A fundamental physical parameter for studying the impact of sunlit, solar and geomagnetic activity on the upper ionosphere and its coupling with the magnetosphere is the electron temperature. This quantity exhibits distinct features with spatial, diurnal, seasonal and activity variability [64–71]. Pignalberi et al. [72] performed a statistical and global study of the electron temperature in the topside ionosphere derived from seven years of in situ data acquired by the Swarm mission at 1 s cadence. The results obtained with this unprecedented data set were compared to data modelled by the International Reference Ionosphere (IRI) model, as well as data obtained from incoherent scatter radars (ISRs). This also allowed an understanding of the deviation between the IRI model and the measurements and testing the reliability of including Swarm data in the empirical data set layer of the IRI itself. Finally, the authors showed that adding the Lomidze calibration to Swarm data [73] improved their agreement with ISR data and the IRI model, especially at mid-latitudes and during the daytime. Another significant parameter representative of the ionosphere is the equivalent slab thickness (EST), i.e., the ration of the TEC to the NmF2. By definition, this parameter represents an imaginary equivalent depth of the ionosphere and includes information on both the topside and bottomside ionosphere, thus being useful in the study of variations in the upper atmosphere (see, e.g., [74-76]). EST exhibits diurnal, seasonal solar and geomagnetic activity variations with a dependence on the location of the observing station. The greatest variability is observed during periods of geomagnetic storms. Zhang et al. [77] analysed the EST in Guam, at equatorial latitudes, confirming and discussing previous results in the literature. In addition, they obtained some new results pointing out diurnal and seasonal changes and the effect of geomagnetic storms on EST at the magnetic equator. In particular, they found that during positive storms, the penetration electric field increases plasma uplift, causing an increase in TEC accompanied by small increases in NmF2. Moreover, equatorward winds drive plasma into the topside ionosphere at the equator resulting in TEC that does not undergo severe depletion like NmF2 does during negative storms. Thus, geomagnetic storms enhance EST both during positive and negative storms.

The monitoring of the physical properties of the ionosphere and their perturbation also has applications in the study of phenomena that can be considered as precursors of Remote Sens. 2022, 14, 5325 5 of 8

major seismic events. Since the early work of Moore [78] and Davies & Baker [79], the idea was proposed that the processes of earthquake preparation and occurrence could be linked to ionospheric disturbances due to lithosphere-atmosphere-ionosphere coupling. With the increase in available data, this idea has become more and more widespread, and in the last decades, new satellite missions have been conceived to monitor natural disaster activities (QuakeSat, SICH-1M, COMPASS-2, DEMETER, CSES). Satellites with other declared purposes, such as the European Space Agency's Swarm constellation, have also provided important information for ionospheric disturbances. Recently, several works investigated magnetic field anomalies observed by both ground and space facilities to study the lithosphere–atmosphere–ionosphere coupling effects of earthquakes [80–82]. In this context, deep learning techniques are used to carry out statistical studies based on the analysis of large numbers of earthquakes. Xiong et al. [83] proposed a deep learning framework for pre-earthquake ionospheric perturbation identification model called SafeNet, which performs better in identifying possible pre-earthquake ionospheric anomalies the more intense the earthquakes are. Ionospheric scintillations are also used for correlations with the occurrence of earthquakes. Some studies in the literature pointed out that thermal expansion of the atmosphere derived from land surface temperature increase before earthquakes can generate small gravity waves altering the electron density profile and causing changes in the TEC, and, on the other hand, ionospheric perturbations can be detected in the hours after large earthquakes [84,85] (Tsugawa et al. 2011, Pavilidou et al. 2019). Few works in the literature investigated the correlation between the occurrence of earthquakes and ionospheric scintillation (see, e.g., [86]). These studies take advantage of GPS data from ground stations or ionosondes to measure the scintillation index S4 and study its correlation with earthquakes in the same region. By using statistical tools, Molina et al. [87] for the first time used the GNSS reflectometry [88] technique to obtain global oceanic maps of ionospheric scintillation and correlate them to earthquake precursors. Their results point out a small positive correlation for earthquakes with magnitudes above 4, with better results for increasing magnitudes. Correlation was better when positive increments in the S4 index were observed between 6 and 3 days before the earthquakes than the ones observed after them. In the best case, the correct prediction probability is about 32% and the false alarm probability is 16%; however, the probability of detection is small overall. The authors also recognise that the signature of ionospheric scintillation increments as precursors of earthquakes is still small and should not be regarded as an early warning system for earthquakes.

Funding: This research received no external funding.

Conflicts of Interest: The authors declare no conflict of interest.

References

1. Shindin, A.V.; Sergey, P.M.; Vybornov, F.I.; Grechneva, K.K.; Pavlova, V.A.; Khashev, V.R. The Prototype of a Fast Vertical Ionosonde Based on Modern Software-Defined Radio Devices. *Remote Sens.* **2022**, *14*, 547. [CrossRef]

- 2. Pietrella, M.; Bianchi, C. Occurrence of sporadic-E layer over the ionospheric station of Rome: Analysis of data for thirty-two years. *Adv. Space Res.* **2009**, *44*, 72–81. [CrossRef]
- 3. Haldoupis, C.; Pancheva, D.; Singer, W.; Meek, C.; Macdougall, J. An explanation for the seasonal dependence of midlatitude sporadic E layers. *J. Geophys. Res.* **2007**, *112*, A6.
- 4. Whitehead, J.D. Formation of the sporadic E layer in the temperate zones. J. Atmos. Terr. Phys. 1961, 20, 49–58. [CrossRef]
- 5. Axford, W.; Cunnold, D. The wind shear theory of temperate zone sporadic E. Radio Sci. 1966, 1, 191–197. [CrossRef]
- 6. Nygrén, T.; Lanchester, B.S.; Huuskonen, A.; Jalonen, L.; Eyken, A. Interference of tidal and gravity waves in the ionosphere and an associated sporadic E-layer. *J. Atmos. Sol.-Terr. Phys.* **1990**, *52*, 609–623. [CrossRef]
- 7. Goldsbrough, P.F.; Ellyett, C.D. Relationship of meteors to sporadic E, 2. statistical evidence for class 1 Em. *J. Geophys. Res. Atmos.* **1976**, *81*, 6135–6140. [CrossRef]
- 8. Barta, V.; Haldoupis, C.; Sátori, G.; Buresova, D.; Bencze, P. Searching for effects caused by thunderstorms in midlatitude sporadic E layers. *J. Atmos. Sol.-Terr. Phys.* **2017**, *161*, 150–159. [CrossRef]
- 9. Mori, H.; Oyama, K.I. Sounding rocket observation of sporadic-E layer electron-density irregularities. *Geophys. Res. Lett.* **1998**, 25, 1785–1788. [CrossRef]

Remote Sens. 2022, 14, 5325 6 of 8

10. Mori, H.; Oyama, K.I. Rocket observation of sporadic-E layers and electron density irregularities over midlatitude. *Adv. Space Res.* **2000**, *26*, 1251–1255. [CrossRef]

- 11. Bernhardt, P.A.; Selcher, C.A.; Siefring, C.; Wilkens, M.; Compton, C.; Bust, G.; Yamamoto, M.; Fukao, S.; Takayuki, O.; Wakabayashi, M. Radio tomographic imaging of sporadic-E layers during SEEK-2. *Ann. Geophys.* **2005**, *23*, 2357–2368. [CrossRef]
- 12. Damtie, B.; Nygrén, T.; Lehtinen, M.S.; Huuskonen, A. High resolution observations of sporadic-E layers within the polar cap ionosphere using a new incoherent scatter radar experiment. *Ann. Geophys.* **2003**, *20*, 1429–1438. [CrossRef]
- 13. Turunen, T.; Nygrén, T.; Huuskonen, A.; Jalonen, L. Incoherent scatter studies of sporadic-E using 300 m resolution. *J. Atmos. Terr. Phys.* **1988**, *50*, 277–287. [CrossRef]
- 14. Liu, T.; Yang, G.; Zhou, C.; Jiang, C.; Xu, W.; Ni, B.; Zhao, Z. Improved Ionosonde Monitoring of the Sporadic E Layer Using the Frequency Domain Interferometry Technique. *Remote Sens.* **2022**, *14*, 1915. [CrossRef]
- 15. Smith, M.S. The calculation of ionospheric profiles from data given on oblique incidence ionograms. *J. Atmos. Terr. Phys.* **1970**, 32, 1047–1056. [CrossRef]
- 16. Chen, J.; Bennett, J.A.; Dyson, P.L. Synthesis of oblique ionograms from vertical ionograms using quasi-parabolic segment models of the ionosphere. *J. Atmos. Terr. Phys.* **1992**, *54*, 323–331. [CrossRef]
- 17. Phanivong, B.; Chen, J.; Dyson, P.L.; Bennett, J.A. Inversion of oblique ionograms including the earth's magnetic field. *J. Atmos. Sol. Terr. Phys.* **1995**, *57*, 1715–1721. [CrossRef]
- 18. Huang, X.; Reinisch, B.W.; Kuklinski, W.S. Mid-point electron density profiles from oblique ionograms. *Ann. Geophys. Italy* **1996**, 49, 757–761. [CrossRef]
- 19. Redding, N.J. Image understanding of oblique ionograms: The autoscaling problem. In Proceedings of the IEEE Australian and New Zealand Conference on Intelligent Information Systems, Adelaide, SA, Australia, 18–20 November 1996; IEEE: Piscataway, NJ, USA, 1996; pp. 155–160.
- 20. Fan, J.; Lu, Z.; Jiao, P. The intelligentized recognition of oblique propagation modes. Chin. J. Radio Sci. 2009, 24, 528. (In Chinese)
- 21. Settimi, A.; Pezzopane, M.; Pietrella, M.; Bianchi, C.; Scotto, C.; Zuccheretti, E.; Makris, J. Testing the IONORT-ISP system: A comparison between synthesized and measured oblique ionograms. *Radio Sci.* **2013**, *48*, 167–179. [CrossRef]
- 22. Ippolito, A.; Scotto, C.; Francis, M.; Settimi, A.; Cesaronl, C. Automatic interpretation of oblique ionograms. *Adv. Space Res.* **2015**, 55, 1624–1629. [CrossRef]
- 23. Heitmann, A.J.; Gardiner-Garden, R.S. A robust feature extraction and parameterized fitting algorithm for bottom-side oblique and vertical incidence ionograms. *Radio Sci.* **2019**, *54*, 115–134. [CrossRef]
- 24. Jiang, C.; Zhao, C.; Zhang, X.; Liu, T.; Chen, Z.; Yang, G.; Zhao, Z. A Method for Automatic Inversion of Oblique Ionograms. *Remote Sens.* **2022**, *14*, 1671. [CrossRef]
- 25. Kim, E.; Jee, G.; Ham, Y.-B.; Zabotin, N.; Lee, C.; Kwon, H.-J.; Hong, J.; Kim, J.-H.; Bullett, T. Assessment of Polar Ionospheric Observations by VIPIR/Dynasonde at Jang Bogo Station, Antarctica: Part 1—Ionospheric Densities. *Remote Sens.* 2022, 14, 2785. [CrossRef]
- 26. Hocking, W.K.; Fukao, S.; Tsuda, T.; Yamamoto, M.; Sato, T.; Kato, S. Aspect sensitivity of stratospheric VHF radar wave scatterers, particularly above 15-km altitude. *Radio Sci.* **1990**, 25, 613–627. [CrossRef]
- 27. Chen, J.-S.; Furumoto, J. Measurement of atmospheric aspect sensitivity using coherent radar imaging after mitigation of radar beam weighting effect. *J. Atmos. Ocean. Technol.* **2013**, *30*, 245–259. [CrossRef]
- 28. Kudeki, E.; Farley, D. Aspect sensitivity of equatorial electrojet irregularities and theoretical implications. *J. Geophys. Res.* **1989**, *94*, 426–434. [CrossRef]
- 29. Farley, D.T.; Hysell, D.L. Radar measurement of very small aspect angles in the equatorial ionosphere. *J. Geophys. Res.* **1996**, *101*, 5177–5184. [CrossRef]
- 30. Chen, J.-S.; Wang, C.-Y.; Chu, Y.-H. Measurement of Aspect Angle of Field-Aligned Plasma Irregularities in Mid-Latitude E Region Using VHF Atmospheric Radar Imaging and Interferometry Techniques. *Remote Sens.* **2022**, *14*, 611. [CrossRef]
- 31. Palmer, R.D.; Gopalam, S.; Yu, T.-Y.; Fukao, S. Coherent radar imaging using Capon's method. *Radio Sci.* 1998, 33, 1585–1598. [CrossRef]
- Karpachev, A. Advanced Classification of Ionospheric Troughs in the Morning and Evening Conditions. Remote Sens. 2022, 14, 4072. [CrossRef]
- 33. Kil, H.; Heelis, R.A. Global distribution of density irregularities in the equatorial ionosphere. *J. Geophys. Res. (Space Phys.)* **1998**, 103, 407–418. [CrossRef]
- 34. Kelley, M.C. The Earth's Ionosphere: Plasma Physics and Electrodynamics, 2nd ed.; Academic Press: Burlington, MA, USA, 2009.
- 35. Anderson, D.N.; Mendillo, M. Ionospheric conditions affecting the evolution of equatorial plasma depletions. *Geophys. Res. Lett.* **1983**, *10*, 541–544. [CrossRef]
- 36. Tsunoda, R.T.; Livingston, R.C.; McClure, J.P.; Hanson, W.B. Equatorial plasma bubbles: Vertically elongated wedges from the bottomside F layer. *J. Geophys. Res. (Space Phys.)* **1982**, *87*, 9171–9180. [CrossRef]
- 37. Smith, J.; Heelis, R.A. Equatorial plasma bubbles: Variations of occurrence and spatial scale in local time, longitude, season, and solar activity. *J. Geophys. Res.* (*Space Phys.*) **2017**, 122, 5743–5755. [CrossRef]
- 38. Gurram, P.; Kakad, B.; Bhattacharyya, A.; Pant, T.K. Evolution of Freshly Generated Equatorial Spread F (F-ESF) Irregularities on Quiet and Disturbed Days. *J. Geophys. Res. (Space Phys.)* **2018**, *123*, 7710–7725. [CrossRef]
- 39. Schunk, R.; Nagy, A. Ionospheres: Physics, Plasma Physics, and Chemistry; Cambridge University Press: Cambridge, UK, 2009.

Remote Sens. 2022, 14, 5325 7 of 8

- 40. Kraichnan, R.H. Inertial Ranges in Two-Dimensional Turbulence. Phys. Fluids 1967, 10, 1417–1423. [CrossRef]
- 41. Kraichnan, R.H.; Montgomery, D. Two-dimensional turbulence. Rep. Prog. Phys. 1980, 43, 547-619. [CrossRef]
- 42. McDaniel, R.D.; Hysell, D.L. Models and DE II observations of inertial-regime irregularities in equatorial spread F. J. Geophys. Res. (Space Phys.) 1997, 102, 22233–22246. [CrossRef]
- 43. Yokoyama, T.; Shinagawa, H.; Jin, H. Nonlinear growth, bifurcation, and pinching of equatorial plasma bubble simulated by three-dimensional high-resolution bubble model. *J. Geophys. Res. (Space Phys.)* **2014**, *119*, 10474–10482. [CrossRef]
- 44. Yokoyama, T. A review on the numerical simulation of equatorial plasma bubbles toward scintillation evaluation and forecasting. *Prog. Earth Planet. Sci.* **2017**, *4*, 37. [CrossRef]
- 45. Hysell, D.L.; Shume, E.B. Electrostatic plasma turbulence in the topside equatorial F region ionosphere. *J. Geophys. Res.* (*Space Phys.*) **2002**, 107, 1269. [CrossRef]
- 46. De Michelis, P.; Consolini, G.; Alberti, T.; Tozzi, R.; Giannattasio, F.; Coco, I.; Pezzopane, M.; Pignalberi, A. Magnetic Field and Electron Density Scaling Properties in the Equatorial Plasma Bubbles. *Remote Sens.* **2022**, *14*, 918. [CrossRef]
- 47. Lühr, H.; Rother, M.; Maus, S.; Mai, W.; Cooke, D. The diamagnetic effect of the equatorial Appleton anomaly: Its characteristics and impact on geomagnetic field modeling. *Geophys. Res. Lett.* **2003**, *30*, 1906. [CrossRef]
- 48. De Michelis, P.; Consolini, G.; Tozzi, R. Magnetic field fluctuation features at Swarm's altitude: A fractal approach. *Geophys. Res. Lett.* **2015**, 42, 3100–3105. [CrossRef]
- 49. Lovati, G.; De Michelis, P.; Consolini, G.; Berrilli, F. Pressure-Gradient Current at High Latitude from Swarm Measurements. *Remote Sens.* **2022**, *14*, 1428. [CrossRef]
- 50. Kintner, P.M., Jr. Observations of velocity shear driven plasma turbulence. J. Geophys. Res. 1976, A28, 5114-5122. [CrossRef]
- 51. Kintner, P.M.; Seyler, C.E. The status of observations and theory of high latitude ionospheric and magnetospheric plasma turbulence. *Space Sci. Rev.* **1985**, *41*, 1572–9672. [CrossRef]
- 52. Basu, S.; Basu, S.; MacKenzie, E.; Fougere, P.F.; Coley, W.R.; Maynard, N.C.; Winningham, J.D.; Sugiura, M.; Hanson, W.B.; Hoegy, W.R. Simultaneous density and electric field fluctuation spectra associated with velocity shears in the auroral oval. *J. Geophys. Res. Space Phys.* 1988, 93, 115–136. [CrossRef]
- 53. Kozelov, B.V.; Golovchanskaya, I.V.; Ostapenko, A.A.; Fedorenko, Y.V. Wavelet analysis of high-latitude electric and magnetic fluctuations observed by the Dynamic Explorer 2 satellite. *J. Geophys. Res. Space Phys.* **2008**, *113*, A03308. [CrossRef]
- 54. Fejer, B.G.; Kelley, M.C. Ionospheric irregularities. Rev. Geophys. Space Phys. 1980, 18, 401–454. [CrossRef]
- 55. Fejer, B.G. Low latitude electrodynamic plasma drifts—A review. J. Atmos. Terr. Phys. 1991, 53, 677–693. [CrossRef]
- 56. Anderson, D.; Anghel, A.; Yumoto, K.; Ishitsuka, M.; Kudeki, E. Estimating daytime vertical ExB drift velocities in the equatorial F-region using ground-based magnetometer observations. *Geophys. Res. Lett.* **2002**, *29*, 1596. [CrossRef]
- 57. Consolini, G.; Quattrociocchi, V.; Benella, S.; De Michelis, P.; Alberti, T.; Piersanti, M.; Marcucci, M.F. On Turbulent Features of E × B Plasma Motion in the Auroral Topside Ionosphere: Some Results from CSES-01 Satellite. *Remote Sens.* **2022**, 14, 1936. [CrossRef]
- 58. Gao, Z.; Fang, K.; Zhu, Y.; Wang, Z.; Guo, K. An Ionospheric Anomaly Monitor Based on the One Class Support Vector Algorithm for the Ground-Based Augmentation System. *Remote Sens.* **2021**, *13*, 4327. [CrossRef]
- 59. Valdés-Abreu, J.C.; Díaz, M.A.; Bravo, M.; Báez, J.C.; Stable-Sánchez, Y. Ionospheric Behavior during the 10 June 2021 Annular Solar Eclipse and Its Impact on GNSS Precise Point Positioning. *Remote Sens.* **2022**, *14*, 3119. [CrossRef]
- 60. Bravo, M.; Martínez-Ledesma, M.; Foppiano, A.; Urra, B.; Ovalle, E.; Villalobos, C.; Souza, J.; Carrasco, E.; Muñoz, P.R.; Tamblay, L.; et al. First Report of an Eclipse from Chilean Ionosonde Observations: Comparison with Total Electron Content Estimations and the Modeled Maximum Electron Concentration and Its Height. *J. Geophys. Res. Space Phys.* 2020, 125, e2020JA027923. [CrossRef]
- 61. Le, H.; Liu, L.; Yue, X.; Wan, W. The ionospheric behavior in conjugate hemispheres during the 3 October 2005 solar eclipse. *Ann. Geophys.* **2009**, 27, 179–184. [CrossRef]
- 62. He, L.; Heki, K.; Wu, L. Three-Dimensional and Trans-Hemispheric Changes in Ionospheric Electron Density Caused by the Great Solar Eclipse in North America on 21 August 2017. *Geophys. Res. Lett.* **2018**, *45*, 10933–10940. [CrossRef]
- 63. Aa, E.; Zhang, S.R.; Shen, H.; Liu, S.; Li, J. Local and conjugate ionospheric total electron content variation during the 21 June 2020 solar eclipse. *Adv. Space Res.* **2021**, *68*, 3435–3454. [CrossRef]
- 64. Willmore, A.P. Electron and ion temperatures in the ionosphere. Space Sci. Rev. 1970, 11, 607–670. [CrossRef]
- 65. Rishbeth, H.; Garriott, O. *Introduction to Ionospheric Physics*; International Geophysics Series v. 14; Academic Press: New York, NY, USA, 1969.
- 66. Ratcliffe, J.A. An Introduction to the Ionosphere and Magnetosphere; Cambridge University Press: Cambridge, UK, 1972.
- 67. Banks, P.M. Ion temperature in the upper atmosphere. J. Geophys. Res. Space Phys. 1967, 72, 3365–3385.
- 68. Roble, R. The calculated and observed diurnal variation of the ionosphere over Millstone Hill on 23–24 March 1970. *Planet. Space Sci.* **1975**, 23, 1017–1033. [CrossRef]
- 69. Schunk, R.W.; Nagy, A.F. Electron temperatures in the region of the ionosphere: Theory and observations. *Rev. Geophys.* **1978**, *16*, 355–399. [CrossRef]
- 70. Bilitza, D. Electron and ion temperature data for ionospheric modelling. Adv. Space Res. 1991, 11, 139–148. [CrossRef]
- 71. Evans, J. Theory and practice of ionosphere study by Thomson scatter radar. Proc. IEEE 1969, 57, 496–530. [CrossRef]

Remote Sens. 2022, 14, 5325 8 of 8

72. Pignalberi, A.; Giannattasio, F.; Truhlik, V.; Coco, I.; Pezzopane, M.; Consolini, G.; De Michelis, P.; Tozzi, R. On the Electron Temperature in the Topside Ionosphere as Seen by Swarm Satellites, Incoherent Scatter Radars, and the International Reference Ionosphere Model. *Remote Sens.* **2021**, *13*, 4077. [CrossRef]

- 73. Lomidze, L.; Knudsen, D.J.; Burchill, J.; Kouznetsov, A.; Buchert, S.C. Calibration and validation of swarm plasma densities and electron temperatures using ground-based radars and satellite radio occultation measurements. *Radio Sci.* **2018**, *53*, 15–36. [CrossRef]
- 74. Maltseva, O.A.; Mozhaeva, N.S.; Nikitenko, T.V. Comparison of model and experimental ionospheric parameters at high latitudes. *Adv. Space Res.* **2013**, *51*, 599–609. [CrossRef]
- 75. Maltseva, O.A.; Mozhaeva, N.S.; Nikitenko, T.V. Validation of the Neustrelitz Global Model according to the low latitude ionosphere. *Adv. Space Res.* **2014**, *54*, 463–472. [CrossRef]
- 76. Maltseva, O.A.; Mozhaeva, N.S. The Use of the Total Electron Content Measured by Navigation Satellites to Estimate Ionospheric Conditions. *Int. J. Navig. Obs.* **2016**, 2016, 7016208. [CrossRef]
- 77. Zhang, Y.; Wu, Z.; Feng, J.; Xu, T.; Deng, Z.; Ou, M.; Xiong, W.; Zhen, W. Statistical Study of Ionospheric Equivalent Slab Thickness at Guam Magnetic Equatorial Location. *Remote Sens.* **2021**, *13*, 5175. [CrossRef]
- 78. Moore, G.W. Magnetic Disturbances preceding the 1964 Alaska Earthquake. Nature 1964, 203, 508–509. [CrossRef]
- 79. Davies, K.; Baker, D.M. Ionospheric effects observed around the time of the Alaskan earthquake of March 28, 1964. *J. Geophys. Res.* 1965, 70, 2251–2253. [CrossRef]
- 80. De Santis, A.; Balasis, G.; Pavón-Carrasco, F.J.; Cianchini, G.; Mandea, M. Potential earthquake precursory pattern from space: The 2015 Nepal event as seen by magnetic Swarm satellites. *Earth Planet. Sci. Lett.* **2017**, *461*, 119–126. [CrossRef]
- 81. Marchetti, D.; De Santis, A.; D'Arcangelo, S.; Poggio, F.; Piscini, A.; Campuzano, S.A.; De Carvalho, W.V.J.O. Pre-earthquake chain processes detected from ground to satellite altitude in preparation of the 2016–2017 seismic sequence in Central Italy. *Remote Sens. Environ.* **2019**, 229, 93–99. [CrossRef]
- 82. Zhu, K.; Fan, M.; He, X.; Marchetti, D.; Li, K.; Yu, Z.; Chi, C.; Sun, H.; Cheng, Y. Analysis of Swarm Satellite Magnetic Field Data Before the 2016 Ecuador (Mw = 7.8) Earthquake Based on Non-negative Matrix Factorization. *Front. Earth Sci.* **2021**, 9, 1976. [CrossRef]
- 83. Xiong, P.; Marchetti, D.; De Santis, A.; Zhang, X.; Shen, X. SafeNet: SwArm for Earthquake Perturbations Identification Using Deep Learning Networks. *Remote Sens.* **2021**, *13*, 5033. [CrossRef]
- 84. Tsugawa, T.; Saito, A.; Otsuka, Y.; Nishioka, M.; Maruyama, T.; Kato, H.; Nagatsuma, T.; Murata, K.T. Ionospheric disturbances detected by GPS total electron content observation after the 2011 off the Pacific coast of Tohoku Earthquake. *Earth Planets Space* **2011**, 63, 875–879. [CrossRef]
- 85. Pavlidou, E.; Van der Meijde, M.; Van der Werff, H.; Hecker, C. Time Series Analysis of Land Surface Temperatures in 20 Earthquake Cases Worldwide. *Remote Sens.* **2019**, *11*, 61. [CrossRef]
- 86. Kandalyan, R.A.; AlQuran, M.K. Ionosphere scintillation and earthquakes. Jordan J. Phys. 2010, 3, 69–76.
- 87. Molina, C.; Boudriki Semlali, B.-E.; Park, H.; Camps, A. A Preliminary Study on Ionospheric Scintillation Anomalies Detected Using GNSS-R Data from NASA CYGNSS Mission as Possible Earthquake Precursors. *Remote Sens.* **2022**, *14*, 2555. [CrossRef]
- 88. Camps, A.; Park, H.; Foti, G.; Gommenginger, C. Ionospheric Effects in GNSS-Reflectometry from Space. *IEEE J. Sel. Top. Appl. Earth Obs. Remote Sens.* **2016**, *9*, 5851–5861. [CrossRef]